ChemElectroChem

Articles
doi.org/10.1002/celc.202001146

Chemistry Europe
European Chemical
Societies Publishing

Analysis of the Capacitive Behavior of Polymer Electrolyte Membrane Fuel Cells during Operation

Tim Lochner,*[a, b] Markus Perchthaler,[a] Franziska Hnyk,[a] Daniel Sick,[a] Jarek P. Sabawa,[a] and Aliaksandr S. Bandarenka*[b, c]

The interest in polymer electrolyte membrane fuel cells for automotive applications is nowadays increasing. To run such systems efficiently, the operating strategy relies on information about the stacks operational conditions. The cell capacitance, in most cases, contains such information and it can be measured in real-time using electrochemical impedance spectroscopy. However, the influence of the operating conditions on the cell capacitance is poorly understood so far. Therefore, this work analyses the influence of the oxygen content and cell voltage.

Cyclic voltammetry and impedance spectroscopy data show equal hydrogen adsorption charges in oxygen-free operation. In oxygen-saturated atmosphere, the adsorption capacitance below 0.40 V is suppressed, probably owing to the fast adsorption of OH*. However, this allows distinction between the oxygen-free and oxygen-saturated conditions, as in the first case the total capacitance is significantly larger. Thus, an impedance-based operation strategy could detect oxygen undersupply in the fuel cells in real-time.

1. Introduction

The BMW Group is "convinced that various alternative power-train systems will exist alongside one another in future, as there is no single solution that addresses the full spectrum of customers' mobility requirements worldwide".[1] Polymer electrolyte membrane fuel cell (PEMFC) technology is one of these alternative powertrain systems. For a successful market introduction, an operational strategy is needed that is able to control e.g. air and hydrogen flows, membrane humidification and power output. Optimal operational strategies increase system performance, reliability and lifetime and should, therefore, rely on real-time information on the current fuel cell's state. Electrochemical impedance spectroscopy (EIS) is a tool to monitor such states and possible faults during the operation[2–8] by modulating the stack current using e.g. a DC/DC converter.[9,10] An impedance measurement can give the information about resistive, inductive and capacitive characteristics of the fuel cell stacks. To date, monitoring of fuel cells focuses on the resistive response, which is mainly influenced by

the membrane hydration,[11] Tafel characteristics[12] and adsorption resistances.[13] System malfunctions such as an oxygen shortage are typically identified based on the resistive phenomena,[14,15,16] while the capacitive behavior is often neglected. However, the capacitive response contains important information on the electrode degradation[17] and state of operation.[18] EIS measures the so-called differential capacitance $C = \partial q/\partial U$, where q is the charge and U is the voltage. The change of electrical charges at the interface ∂q with voltage ∂U can arise from the double layer charging and specific adsorption processes.[13,19,20] The cell capacitance during the operation is dependent on many parameters, such as voltage, temperature, hydrogen and oxygen partial pressure as well as membrane humidification, just to mention a few.[21–23]

Only several studies have focused on the capacitive behavior of fuel cells under oxygen-saturated and oxygen-depleted operational conditions. While some authors observe variations in the capacitance in different operational modes,[21–23] the physical origins of these variations remain unclear. In oxygen-depleted operation (nitrogen at the cathode), cyclic voltammetry (CV) reveals changes in the cell capacitance due to hydrogen adsorption/desorption and OH-layer formation dependent on the electrode potential. Since PEMFC cathodes operate with oxygen, the capacitive characteristics at various oxygen contents at the cathode are of interest for automotive applications.

This work analyses the impact of voltage and oxygen partial pressure on the capacitive impedance response in the lab- and automotive-size PEMFCs. The investigated potential range, oxygen partial pressures and materials were those relevant for automotive applications. EIS is used to measure the fuel cell capacitances at the oxygen contents between 0 vol.% and 21 vol.% at potentials from 0.08 V to 0.90 V assuming stationary operation conditions. It is demonstrated that the monitoring of the PEMFCs via EIS is also advantageous for the assessment of

[a] T. Lochner, Dr. M. Perchthaler, F. Hnyk, D. Sick, J. P. Sabawa
BMW Group
80809 München, Germany
E-mail: tim.lochner@bmw.de
[b] T. Lochner, Prof. A. S. Bandarenka
Physik-Department ECS
Technische Universität München
James-Franck-Str. 1, 85748 Garching, Germany
E-mail: bandarenka@ph.tum.de
[c] Prof. A. S. Bandarenka
Catalysis Research Center
Technical University of Munich
Ernst-Otto-Fischer-Str. 1, 85748 Garching, Germany

ChemElectroChem

Articles
doi.org/10.1002/celc.202001146

Chemistry Europe
European Chemical
Societies Publishing

the PEMFC under operational conditions, which is important for automotive applications.[24–27]

Experimental Section

Cell Setup

The experiments were conducted using two lab and two automotive size membrane electrode assemblies (MEAs) with an active area of 43.56 cm^2 (Figure 1A) and 285 cm^2 (Figure 1B), respectively. The cathode catalyst loading of all the test items were similar. The polymer electrolyte membrane of every MEA had a thickness of 15 μm. The catalyst-coated membranes were placed between the gas diffusion layers (types: 29BC at the anode and 22BB at the cathode) provided by SGL Carbon (Table 1). The flow field was pressed into the metallic bipolar plates for the automotive size test items. The flow field of the lab size cells was milled into the graphitic bipolar plates. The setup of MEA #3 (see Table 1) was additionally equipped with a current density distribution measurement unit, provided by S++ Simulation Services. This device allowed measuring the electrical current with a spatial resolution of 0.54 cm^2 (in total 576 segments) and was located near the cathode electrode.[28] The developed analysis approach was intended to be independent on the PEMFC type and setup. It is therefore important to mention that there are differences in flow fields and catalyst type between MEAs #1 to #4.
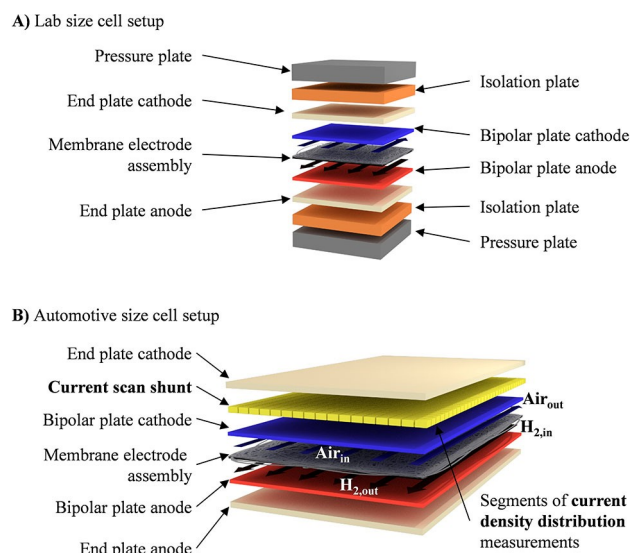

Figure 1. Schematic representation of the cell setup for **A)** the lab size and **B)** the automotive size **test** items.

Fuel Cell Operation

The fuel cells were operated stationary in a potentiostatic mode between 0.080 V and 0.865 V. The corresponding parameters are listed in Table 2. The anode was supplied with hydrogen (purity 99.999 % provided by Linde Gas). The cathode was fed with nitrogen (provided by Linde Gas) or a mixture of nitrogen and air. The volumetric share of oxygen at the cathode ranged between 0 vol.% and 18 vol.%. The anode was treated as the reference electrode during the experiment. To avoid hydrogen starvation, the anode stoichiometry was consistently kept above two. The gas humidification was set to 100 % to avoid dehydration of the polymer membrane and catalyst layer at low currents.

Cyclic Voltammetry

Cyclic voltammograms were measured to determine the charges of the hydrogen underpotential deposition (HUPD), Q_{HUPD}, the electrochemical double layer charging/discharging and the platinum oxidation Q_{Pt-OH}. The CVs were recorded between 0.08 V and 1.0 V with a sweep rate of 30 mV s^{-1}. Five cleaning cycles with a sweep rate of 100 mV s^{-1} removed adsorbates from the Pt surface. 0.40 V was the starting potential to record the CVs. The operational conditions are listed in Table 2. The voltammograms recorded for the MEAs typically show hydrogen evolution at the potentials between 0.0 V and 0.1 V. This distorts the Q_{HUPD} determination. Additionally, a parasitic current across the thin polymer membrane affects the voltammograms. To determine the parasitic and hydrogen evolution currents, CVs at 2.0 mV s^{-1} were recorded. The average currents of the anodic and cathodic sweeps were subtracted from the CVs measured at 30 mV s^{-1}. This is described elsewhere in more detail.[29] All the charges were evaluated during the anodic sweeps (positive currents). The formation of OH* species is thereby calculated between 0.70 V and 1.0 V.

Electrochemical Impedance Spectroscopy

EIS data were recorded under stationary operation conditions. To stabilize the fuel cell operation, each operational parameter set was held for 600 s. Twenty cell voltages between 0.08 V and 0.865 V were analyzed for oxygen volume fractions between 0 vol.% and 18 vol.% for each cell setup. The probing voltage amplitude was set to 20 mV. This rather high amplitude was necessary to minimize the noise but at the same time avoid non-linear effects in the response. The measurement frequencies ranged between 1000 Hz and 0.3 Hz. Complex non-linear least square (CNLS) fitting was performed using the EIS Data Analysis 1.3 software.[30] The fitting results were also verified using differential impedance analysis (DIA). This procedure extracts capacitive information from the impedance data without pre-assuming an equivalent electric circuit (EEC) and, therefore, improves the objectivity of the analysis.[31] In this approach, to calculate the capacitance $C(\omega)$ at a certain measurement frequency ω, the time-constant

Table 1. The active area and the gas diffusion layer type (purchased from SGL Carbon) for the four membrane electrode assemblies analyzed in this study.

ID	Active Area [cm^2]	Gas diffusion layer Cathode	Anode
#1	43.56	22BB	22BB
#2	43.56	22BB	22BB
#3	285	22BB	29BC
#4	285	22BB	29BC

Table 2. Conditions of operation of the fuel cells used in this study. The cell potential and the partial pressure of oxygen at the cathode were varied during the experimental procedures and therefore, they are not listed in this table.

Cell Temperature, °C	60
Anode gas relative humidity inlet, %	100
Cathode gas relative humidity inlet, %	100
Hydrogen volume flow per active area (anode), sccm cm^{-2}	7
Nitrogen volume flow per active area (cathode), sccm cm^{-2}	14.6
Anode gas outlet pressure, bar$_{abs}$	1.5
Cathode gas outlet pressure, bar$_{abs}$	1.05

ChemElectroChem

Articles
doi.org/10.1002/celc.202001146

**Chemistry
Europe**
European Chemical
Societies Publishing

$T(\omega) = \partial L_{eff}(\omega)/\partial Z_{Re}(\omega)$ needs to be calculated based on effective inductance ∂L_{eff} and resistance ∂Z_{Re}. In this work, Eq. 1 is used to determine the cell capacitance.

$$C(\omega) = -\frac{T(\omega)}{\frac{\partial Z_{Re}(\omega)}{\partial \omega} \cdot \frac{(1+\omega^2 T(\omega)^2)^2}{2\omega T(\omega)^2}} \tag{1}$$

The calculation is described in more detail elsewhere.[23]

Current Density Distribution

The current density distribution along the airflow of the cathode was measured using a current scan shunt provided by S++ Simulation Services. A detailed description of the device is given elsewhere.[32] A schematic of the measurement setup is illustrated in Figure 1 B. The current scan shunt is placed between the endplate and BPP of the cathode. To ensure a homogeneous contact pressure between end plate and current scan shunt graphite foils were placed on both sides of the current scan shunt. The current scan shunt consisted of 32×18 segments with a total area of 300 cm^2. Since the active area of the MEA was only 285 cm^2, the segments at the edge of the current scan shunt measured no current and were thus neglected. In this work, the current density distributions are illustrated using 2-dimensional color maps. This way of representation is illustrated in Figure S1 (see supporting information).

2. Results and Discussion

2.1. Capacitance in the Absence of Oxygen

The cyclic voltammogram in Figure 2 A shows three distinct regions. The currents between 0.09 V and 0.40 V are associated with underpotential depositions of hydrogen species (H*). The symmetric peaks at 0.13 V and 0.24 V imply the fast and highly reversible adsorption and desorption of hydrogen. In contrast, the peaks related to the adsorption of OH* species on Pt at potentials between 0.70 V and 1.0 V are asymmetric. Above 0.60 V, the OH-layers form on the Pt surface.[33] The double layer capacitance is evaluated at potentials between 0.40 V and 0.50 V as this range is mainly free of currents related to adsorption processes at the platinum terraces at the surface. Hydrogen evolution causes the peaks below 0.09 V (Figure 2 A). Formation of molecular hydrogen at the cathode can apparently increase the HUPD charge (blue shaded area in Figure 2 A). Performing a background correction, such artifacts can be removed according to Ref. [29].

Impedance data in oxygen free atmosphere were evaluated using the EEC shown in Figure 3 A. It illustrates the model used to fit the data obtained with pure nitrogen at the cathode. The resistance R_{el} describes the Ohmic losses related to the cell setup itself. In the oxygen-free environments, a parallel connection of the double layer capacitance C'_{dl} and the adsorption impedance was used, as described previously using physical modelling.[19,20] The adsorption impedance is a series connection of the resistance R_a and capacitance C_a. To improve the fitting results, a constant phase element Z_a instead of C_a
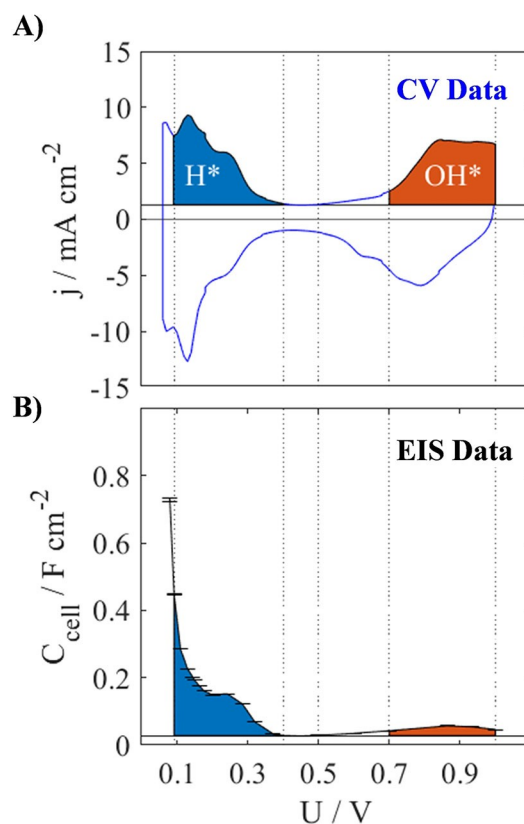

Figure 2. A) A typical cyclic voltammogram of a lab scale PEMFC (MEA #2 in Table 1). B) Cell capacitance values obtained during stationary operation using EIS measurements at different potentials in oxygen free atmosphere. For the CNLS fitting, the equivalent electrical equivalent circuit in Figure 3 A was used. Table 2 lists the corresponding operating conditions.
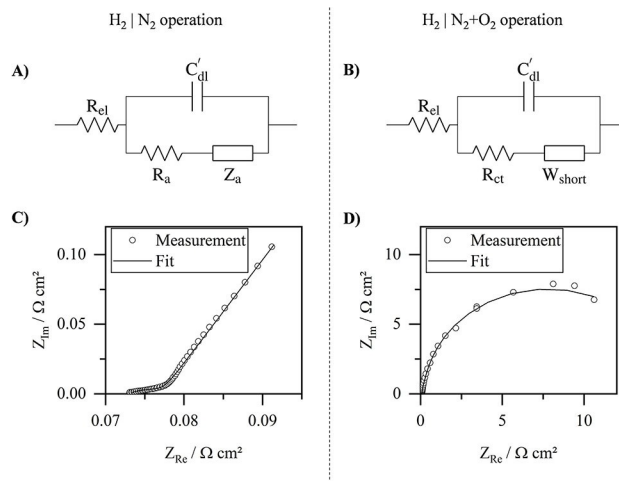

Figure 3. Equivalent electrical circuits (top) and corresponding fitting results (bottom, solid lines). The measurement data were obtained using MEA #1 according to Table 1. The left images (A and C) illustrate the fitting of the impedance data recorded under H$_2$/N$_2$ operation conditions. The right images (B and D) illustrate the fitting of the impedance data recorded under H$_2$/(N$_2$+O$_2$) operation conditions.

was used according to Ref. [34], where $Z_a = Q_a^{-1}(j\omega)^n$. The parameter Q_a is directly proportional to the adsorption

ChemElectroChem

Articles
doi.org/10.1002/celc.202001146

Chemistry Europe
European Chemical
Societies Publishing

capacitance and will be further treated as the capacitance C_a. Some studies show that HUPD influences not only the adsorption but also the measured double layer impedance.[19,20,34] This is due to the high rate constant of hydrogen adsorption: the impedance analysis often cannot separate the fast reversible adsorption/desorption and the double layer charge/discharge. The double layer capacitance C_{dl} is typically assumed constant over the entire potential range.

In the CV (Figure 2 A), it can be seen that almost no adsorption currents occur in the range from 0.40 V to 0.50 V, while some adsorption current in this range can be associated e.g. with the specific adsorption of the OH* species at the under-coordinated sites. Therefore, we determine C_{dl} based on the EIS data also in this area as $C_{dl} = \bar{C}'_{dl}(0.40\ V \leq U \leq 0.50\ V)$. For data presentation, we use the cell capacitance $C_{cell} = C_a + C'_{dl}$ and extract adsorption process by $C_a = C_{cell} - C_{dl}$. C_{cell} is thereby directly comparable to the currents measured by CV. Figure 3 C shows a good agreement between the measured data and the fitting results.

Figure 2 B illustrates the cell capacitance based on the EIS measurements in oxygen free atmosphere as a function of the voltage. The peak at 0.24 V due to hydrogen adsorption is at similar potentials as in the CV. The CV peak at 0.13 V is not present in the impedance data. We assume that the super-imposed voltage oscillation of ±20 mV leads to some hydrogen formation, which can be seen in the CV below 90 mV. For this reason, the EIS measurement at the potentials more negative than 110 mV is overlaid by this effect, which results in an increase of the cell capacitance with the decreasing voltage. The hydrogen adsorption capacitance Q_{HUPD} can be calculated by integrating the $C_a(U)$ curves, and it was calculated to be ~17.5 mC cm^{-2} for MEA #2 (blue shaded area in Figure 2B). This value is similar to ~19.4 mC cm^{-2} calculated based on the CV measurements in Figure 2A. Table 3 compares Q_{HUPD} based on the EIS and CV measurements for all the test items. The EIS analysis shows slightly lower values than in the case of CV, but there is a good correlation between the results.

Similar to the calculation of Q_{HUPD}, the charge was calculated for the OH* adsorption, Q_{Pt-OH}. For MEA #1, Q_{Pt-OH} estimated based on the EIS data was ~8.4 mC cm^{-2}, while the CV measurement gave ~48.9 mC cm^{-2}. Table 3 shows that Q_{Pt-OH} is underestimated in the EIS measurements of all test items due to the irreversibility of the Pt surface oxidation. The formation of an OH-layer leads to a passivation of the catalyst surface. As previously described, this layer formation is a relatively slow process. Due to the stationary mode of operation, the OH-layer forms before the impedance

measurement. In the CV (Figure 2 A) it can be seen that the adsorption and desorption of OH* are differently pronounced at different voltages. Thus, at a voltage above 0.60 V, the application of ±20 mV probing signal changes the catalyst surface only slightly, resulting in lower Q_{Pt-OH} values. Similar trends are observed elsewhere.[19]

2.2. Capacitance in the Presence of Oxygen

EIS is a suitable method to measure the cell capacitance also in the presence of oxygen when the oxygen reduction reaction (ORR) takes place. In this case, the EEC is a parallel combination of the C_{DL} element and elements describing the dominating impedance response of the cathode processes. They can be described using a series connection of the kinetic resistance R_{ct} and a finite length Warburg diffusion element W_{short} (Figure 3B).[13,35] Since this work deals with capacitive effects in the fuel cells, the R_{ct} and W_{short} are not discussed further. Figure 3D shows that the EEC allows accurate data fitting for measurements performed in the presence of the ORR.

Since the addition of oxygen had little influence on Q_{Pt-OH}, we will focus in the following on the potential range of the HUPD (for the full potential range see supporting information Figure S2). The low influence of oxygen on the EEC element values above 0.60 V has already been shown elsewhere.[19] Figure 4 A shows that Q_{HUPD} decreases with increasing oxygen content at the cathode side. This trend was qualitatively visible in all test items. Since Q_{HUPD} in absence of oxygen is different in all cells (see Table 3), no direct comparison of the oxygen content dependence is possible. Therefore, for each MEA we normalized Q_{HUPD} in the presence of oxygen to the respective value without oxygen. These reference values are shown in Table 3 in the column Q_{HUPD} EIS. The dependence of the normalized hydrogen adsorption charge on the oxygen content at the cathode is shown as blue dots in Figure 5A. An exponential decay describes this trend adequately (dashed line in Figure 5A). This shows that all test items also have a qualitatively similar trend. Differences in the behavior can be caused by properties of the flow field, MEA materials, MEA size, etc. and should be investigated in the future. In the HUPD voltage range, no adsorption processes can be measured above an oxygen content of 15 vol.% to 20 vol.% and thus the cell capacitance is equal to the double layer capacitance. However, Figure 4 shows that the peak potential of 0.24 V does not depend on the oxygen content.

Before the previously described behavior is explained in more detail, it is important to rule out the possibility that the EECs (Figure 3) "falsify" the results. The use of equivalent circuits always requires certain assumptions. DIA is one way to calculate the cell capacitance analytically without such presumptions. We, therefore, used it to increase the objectivity of our analysis. Figure 4B shows the cell capacitance obtained based on these calculations. The figure shows the values at 1 Hz based on Eq. 1 as an example, since DIA values are dependent on the measurement frequency. The values over the entire frequency range can be found in the supporting information (Figure S3). Just like the

Table 3. The differential charge within the HUPD region obtained using cyclic voltammetry and electrochemical impedance spectroscopy in H$_2$/N$_2$ (anode/cathode). The IDs correspond to the fuel cell types described in Table 1.

ID	Q_{HUPD} [mC cm^{-2}]		Q_{Pt-OH} [mC cm^{-2}]	
	CV	EIS	CV	EIS
#1	40.3	34.7	48.9	8.4
#2	19.4	17.5	18.5	–
#3	36.3	32.1	46.6	5.8
#4	11.9	10.2	22.6	2.9

These are not the final page numbers! ↗↗

ChemElectroChem

Articles
doi.org/10.1002/celc.202001146

Chemistry Europe
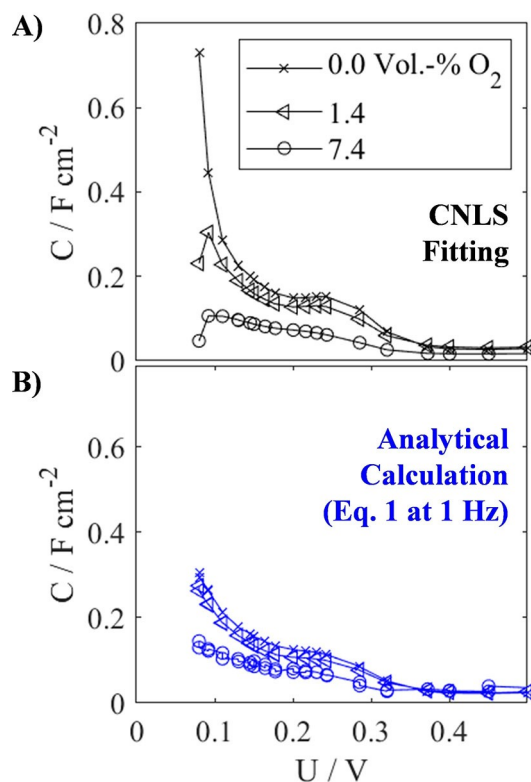European Chemical
Societies Publishing

Figure 4. The differential capacitance of MEA #1 (see Table 1) obtained based on the impedance spectroscopy data analysis as a function of the cathode potential and oxygen content (0, 1.4, 7.4 vol.% O$_2$). A) The CNLS fitting results of the impedance data. B) Differential capacitance values based on analytical processing of the data taken at 1 Hz measurement frequency according to Eq. 1.
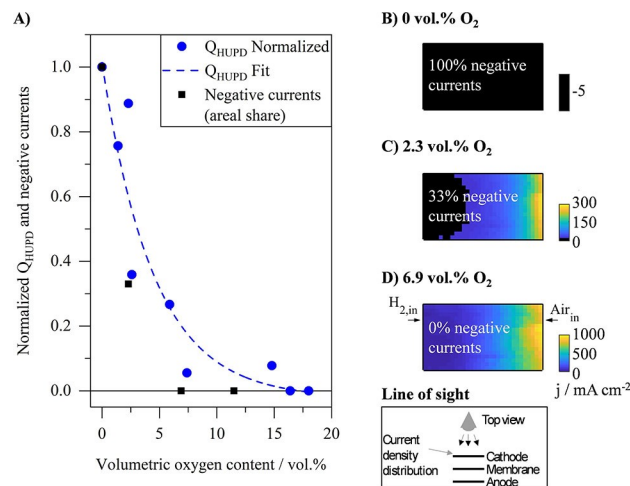

Figure 5. A) The normalized adsorption charge between 0.0 V and 0.40 V (Q_{HUPD}, HUPD region) as a function of the oxygen volume content for four different fuel cell setups (blue dots). To allow a direct comparison of the cell setups, Q_{HUPD} at different oxygen contents is normalized to the Q_{HUPD} value at 0 vol.% O$_2$. An exponential decay equation is fitted to the EIS based data points (blue dashed line). The share of the negative currents in the active area measured by the current density distributions (black squares). The current density distribution maps at 0.24 V for several oxygen contents: B) 0.0 vol.%, C) 2.3 vol.%, and D) 6.9 vol.%. Air and hydrogen flow directions are indicated in (D) and are similar in (B) and (C). The corresponding color bars are shown to the right of the current density distributions. Local negative currents are always shown in black. The inset graph labelled "line of sight" illustrates the position of the current density distribution measurement in the cell setup.

analysis with CNLS fitting, the DIA shows a suppression of Q_{Pt-OH} with increasing the oxygen content.

In order to understand the suppression of Q_{HUPD} in more detail, the current density distribution for different oxygen contents was measured at 0.24 V for the automotive size cell #3 (see Table 1). These are illustrated in Figure 5B to D. We define the currents that flow from the anode to the cathode due to the ORR as positive values. With oxygen contents of 0.0 vol.% (Figure 5B) and 2.3 vol.% (Figure 5C) negative currents occur, which are marked as black areas. The origin of negative currents is hydrogen, which diffuses from the anode through the membrane to the cathode. At the cathode, the hydrogen is oxidized to protons (HOR), which are reduced at the anode. The movement of the electrons is thus opposite to the ORR.

In the absence of oxygen, the currents are negative over the entire active area (Figure 5B). The average current density is −3.6 mA cm^{-2}, which is a typical value for hydrogen crossover at this membrane thickness.[36] Since no oxygen is present, no ORR takes place and therefore no positive currents were measured in Figure 5B. In contrast, at an oxygen content of 6.9 vol.%, the currents within the entire active area are positive (Figure 5D). This is the case, since ORR takes place over the entire area and describes normal fuel cell operation. The current density shows a gradient from the cathode inlet with 1.1 A cm^{-2} to the cathode outlet with 0.069 A cm^{-2}. The average current

density at this operating point is 0.36 A cm^{-2}. The low oxygen content of the supply medium leads to a partial pressure gradient from the inlet to the outlet. Since the ORR depends on the oxygen partial pressure, the current density distribution is dominated by this.

Figure 5 C shows the current density distribution with an oxygen content at the cathode inlet of 2.3 vol.% (at 0.24 V). Starting from the cathode inlet, a decreasing current density can be seen in the direction of the outlet, similar to the measurement at 6.9 vol.%. At 2.3 vol.% oxygen, however, the maximum current density is only at 0.30 A cm^{-2} with an average value of 0.055 A cm^{-2}. Close to the cathode outlet, there are areas with negative currents. Similar to Figure 5B, the cause of the negative currents is the hydrogen crossover. The hydrogen crossover near the air outlet is visible in Figure 5C, since the oxygen is already completely used up in this region. Consequently, at an oxygen content of 2.3 vol.% ORR and HOR take place in parallel in two separate areas within the active area at the cathode. The shares of negative currents in the total area for the respective oxygen contents are shown as black rectangles in Figure 5A.

In the following, we consider the relationship between cell capacitance (blue dots in Figure 5A) and current density distributions (Figure 5B to D). With a nitrogen supply (0 vol.% O$_2$) the MEA has its maximum hydrogen adsorption charge. In that case, the HUPD takes place at the cathode between 0.09 V and 0.40 V:

$$H^+ \leftrightarrow H^* \qquad (2)$$

The (differential) adsorption capacitance $C_a = dq/d\phi$ is larger than zero since the charge at the catalyst surface q changes with the EIS perturbation potential ϕ. From an oxygen content greater than 17 vol.%, C_a is zero, which shows that in the areas where the ORR takes place no adsorption processes contribute significantly to the impedance response in the stationary measurements (Figure 5 A). When supplying oxygen to the cathode the ORR takes place:[37]

$$O_2 \rightarrow {}^*OOH \rightarrow {}^*O \rightarrow {}^*OH \leftrightarrow H_2O \qquad (3)$$
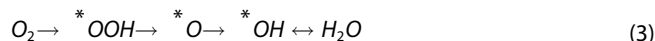
A possible explanation why the adsorption capacitance is zero is that OH* adsorption is very fast at potentials below 0.50 V and cannot be detected by the EIS measurement up to 1 kHz. C_a is therefore zero in locations where the ORR occurs and reaches maximum values in locations with HOR. The maximum value can be extracted from the CV. As soon as HOR and ORR occur in parallel in the cell (Figure 5C), the total capacitance is a mixture of areas with zero and areas with maximum adsorption capacitances. Thus, the quasi-exponential decay in Figure 5A describes the decrease of regions on the active area where an oxygen-depleted atmosphere exists at the cathode.

2.3. Detection of Oxygen Starvation in Fuel Cell Systems

In a fuel cell system, an overall efficiency maximum is one of the main targets. The efficiency optimum is a balance on power production from the fuel cell stack minus the power demand of secondary components, such as coolant pump or air compressor. Thus, the air compressor in a commercial fuel cell system is operated to supply the minimal required airflow for proper cell operation. Several effects might lead to a reactant maldistribution among the induvial cells within a stack.[38] At low air stoichiometries, there is a risk of oxygen starvation which is a typical fault during the operation.[39] In this case, the cathode electrode is at least partially free of oxygen, which is also described in this work.[40] However, an air shortage can also be triggered intentionally to increase the heat production during a freeze start, for example.[41] In the case of a poor air supply, the potential can drop below 0.40 V since the cathode reaction depends strongly on the oxygen partial pressure. The impedance measurements described above demonstrate that in such a case the differential capacitance increases. It has been shown elsewhere that other error cases, such as dehydration of the polymer and the hydrogen undersupply, lead to a collapse of the cell capacitance.[23] Thus, a drop in voltage in combination with an increase in the capacitance can be attributed to the cathode undersupply. This can be relevant for an impedance-based control strategy for PEMFCs. The impedance data detect this effect even at measuring frequencies above 100 Hz (Figure S3), which allows a fast detection of oxygen undersupply.

3. Conclusions

This study presented the results of impedance measurements aiming at the analysis of the capacitive behavior of the automotive and lab size fuel cells. Under oxygen-free operation conditions, EIS shows similar charges of the hydrogen under-potential deposition as CV measurements. During the oxygen-saturated operation, the total capacitance at measurement frequencies below 1 kHz contains only information about the double layer properties but "overlooks" the adsorption processes. Thus, an impedance-based measurement can distinguish between the oxygen-free and oxygen-saturated cells at potentials below 0.40 V. If an MEA is partially supplied with oxygen, two zones with different reactions can form within the active area. In one zone, the ORR takes place as during the fuel cell operation. Within the other zone, the protons are pumped from the cathode to anode side. Thereby, the cell capacitance is between the values found under O_2-free and O_2-saturated operational conditions. Since this effect can be quantified using the impedance-based approaches at frequencies higher than 100 Hz, this is a possible diagnostic tool for fuel cell operation and allows the identification of local and global cathode undersupply in real-time.

Conflict of Interest

The authors declare no conflict of interest.

[1] BMW Group, "The powertrain for the BMW i Hydrogen NEXT: BMW Group reaffirms its ongoing commitment to hydrogen fuel cell technology.", can be found under https://www.press.bmwgroup.com/global/article/detail/T0306930EN/the-powertrain-for-the-bmw-i-hydrogen-next:-bmw-group-reaffirms-its-ongoing-commitment-to-hydrogen-fuel-cell-technology?language=en, **2020**.

[2] N. Fouquet, C. Doulet, C. Nouillant, G. Dauphin-Tanguy, B. Ould-Bouamama, *J. Power Sources* **2006**, *159*, 905–913.

[3] C. Brunetto, A. Moschetto, G. Tina, *Electr. Power Syst. Res.* **2009**, *79*, 17–26.

[4] C. Jeppesen, S. S. Araya, S. L. Sahlin, S. Thomas, S. J. Andreasen, S. K. Kær, *J. Power Sources* **2017**, *359*, 37–47.

[5] N. Fouquet, *2010 IEEE Vehicle Power and Propulsion Conference* **2010**, 1–8.

[6] T. Kurz, A. Hakenjos, J. Krämer, M. Zedda, C. Agert, *J. Power Sources* **2008**, *180*, 742–747.

[7] N. Kitamura, K. Manabe, Y. Nonobe, M. Kizaki, *SAE [Tech. Pap.]* **2010**, DOI 10.4271/2010-01–1088.

[8] A. S. Bandarenka, E. Ventosa, A. Maljusch, J. Masa, W. Schuhmann, *Analyst* **2014**, *139*, 1274–1291.

[9] H.-S. Park, Y.-S. Noh, J.-H. Jegal, S.-H. Baek, B.-J. Kim, C.-Y. Won, *IEEE Transportation Electrification Conference and Expo* **2016**, 386–390.

[10] H. Wang, A. Gaillard, D. Hissel, *Renewable Energy* **2019**, *141*, 124–138.

[11] T. E. Springer, T. A. Zawodzinski, M. S. Wilson, S. Gottesfeld, *J. Electrochem. Soc.* **1996**, *143*, 587–599.

[12] P. Boillat, F. N. Büchi, L. Gubler, T. J. Schmidt, *Meet. Abstr.* **2019**, MA2019-02 1435.

[13] J. P. Sabawa, A. S. Bandarenka, *Electrochim. Acta* **2019**, *311*, 21–29.

[14] F. Mack, R. Laukenmann, S. Galbiati, J. A. Kerres, R. Zeis, *J. Electrochem. Soc.* **2015**, *69*, 1075–1087.

[15] J. O'Rourke, M. Ramani, M. Arcak, *Int. J. Hydrogen Energy* **2008**, *33*, 4694–4701.

[16] J. Zhang, Y. Tang, C. Song, J. Zhang, *J. Power Sources* **2007**, *172*, 163–171.

[17] T. A. Dao, J. Scholta, S. Enz, M. Klages, N. Dannenberg, H. Pommer (Zentrum fuer Sonnenenergie- und Wasserstoff-Forschung, ThyssenKrupp Marine Systems GmbH), EP 3443610 A1, **2017**.

[18] P. Kurzweil, H. J. Fischle, *J. Power Sources* **2004**, *127*, 331–340.

[19] A. S. Bondarenko, I. E. L. Stephens, H. A. Hansen, F. J. Pérez-Alonso, V. Tripkovic, T. P. Johansson, J. Rossmeisl, J. K. Nørskov, I. Chorkendorff, *Langmuir* **2011**, *27*, 2058–2066.

[20] M. D. Pohl, V. Colic, D. Scieszka, A. S. Bandarenka, *Phys. Chem. Chem. Phys.* **2016**, *18*, 10792–10799.

[21] T. Reshetenko, A. Kulikovsky, *RSC Adv.* **2019**, *9*, 38797–38806.

[22] H. Nakajima, T. Kitahara, *Heat Mass Transfer* **2018**, *54*, 2551–2558.

[23] T. Lochner, M. Perchthaler, J. T. Binder, J. P. Sabawa, T. A. Dao, A. S. Bandarenka, *ChemElectroChem* **2020**, *7*, 2784–2791.

[24] T. Ogawa (Toyota Jidosha Kabushiki Kaisha), Y. Naganuma (Toyota Jidosha Kabushiki Kaisha), US 9 793 561 B2, **2017**.

[25] T. H. Min (Hyundai Autron Co., Ltd.), US 9 945 911 B2, **2018**.

[26] M. Matsumoto (Nissan Motor Co., Ltd.), K. Hoshi (Nissan Motor Co., Ltd.), T. Aoki (Nissan Motor Co., Ltd.), US 10 177 391 B2, **2019**.

[27] M. Sinha (GM Global Technology Operations LLC), P. A. Rapaport (GM Global Technology Operations LLC), H. Yoshida (Honda Motor Co., Ltd.), S. Toyota (Honda Motor Co., Ltd.), Y.-H. Lai (GM Global Technology Operations LLC), US 10 218 018 B2, **2019**.

[28] S. Herden, F. Riewald, J. A. Hirschfeld, M. Perchthaler, *J. Power Sources* **2017**, *355*, 36–43.

[29] M. Edmundson, F. C. Busby, *ECS Trans.* **2011**, *41*, 661–671.

[30] A. S. Bandarenka, *Lecture Notes on Impedance Spectroscopy. Measurement, Modeling and Applications*, **2013**, *Vol. 4 (Eds.: O. Kanoun)*, CRC Press, Tailor and Francis Group, London, 29–36.

[31] D. Vladikova, Z. Stoynov, *J. Electroanal. Chem.* **2004**, *572*, 377–387.

[32] R. Kraume, "S++ Simulation Services", can be found under http://www.splusplus.com/, **2007**.

[33] Y. Liu, M. Mathias, J. Zhang, *Electrochem. Solid-State Lett.* **2010**, *13*, B1–B3.

[34] G. A. Ragoisha, N. P. Osipovich, A. S. Bondarenko, J. Zhang, S. Kocha, A. Iiyama, *J. Solid State Electrochem.* **2010**, *14*, 531–542.

[35] M. Itagaki, H. Hasegawa, K. Watanabe, T. Hachiya, *J. Electroanal. Chem.* **2003**, *557*, 59–73.

[36] J. Shan, P. Gazdzicki, R. Lin, M. Schulze, K. A. Friedrich, *Energy* **2017**, *128*, 357–365.

[37] J. Rossmeisl, G. S. Karlberg, T. Jaramillo, J. K. Nørskov, *Faraday Discuss.* **2009**, *140*, 337–346.

[38] M. Mortada, H. S. Ramadan, J. Faraj, A. Faraj, H. El Hage, M. Khaled, *Int. J. Hydrogen Energy* **2020**, DOI: 10.1016/j.ijhydene.2020.06.013.

[39] P. Pei, H. Chen, *Appl. Energy* **2014**, *125*, 60–75.

[40] N. Zamel, R. Hanke-Rauschenbach, S. Kirsch, A. Bhattarai, D. Gerteisen, *Int. J. Hydrogen Energy* **2013**, *38*, 15318–15327.

[41] K. Manabe, Y. Naganuma, Y. Nonobe, M. Kizaki, *SAE [Tech. Pap.]* **2010**, DOI: 10.4271/2010-01-1092.
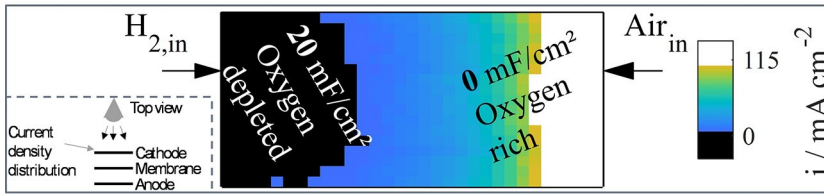
Road to success: The adsorption capacitance of automotive fuel cells is very sensitive to the oxygen content at cell voltages below 0.40 V. This enables impedance-based real-time monitoring of local and global air starvation during vehicle operation.

T. Lochner, Dr. M. Perchthaler, F. Hnyk, D. Sick, J. P. Sabawa, Prof. A. S. Bandarenka**

1 – 8

Analysis of the Capacitive Behavior of Polymer Electrolyte Membrane Fuel Cells during Operation